Parameterization and Observability Analysis of Scalable Battery Clusters for Onboard Thermal Management

Xinfan Lin[1]*, Hector E. Perez[1], Jason B. Siegel[1], Anna G. Stefanopoulou[1],
Yi Ding[2] and Matthew P. Castanier[2]

1 Department of Mechanical Engineering, University of Michigan, Ann Arbor, Michigan, 48109 - USA
2 U.S. Army Tank Automotive Research, Development, and Engineering Center (TARDEC), Warren, Michigan, 48397, USA,
e-mail: xflin@umich.edu - heperez@umich.edu - siegeljb@umich.edu - annastef@umich.edu - yi.ding@us.army.mil -
matt.castanier@us.army.mil
* Corresponding author

Abstract — **Parameterization and Observability Analysis of Scalable Battery Clusters for Onboard Thermal Management** — *Thermal management is an important issue for lithium ion batteries, as overheating may result in disastrous consequences. Although the battery surface temperature is commonly measured, the core temperature of a cell may be much higher hence more critical. The core temperature of a battery, though unmeasurable, can be estimated by an observer, based on a battery thermal model and the measurement of the current and the surface temperature. To enable accurate estimation of the core temperature, the model parameters need to be correctly identified. For such purpose, an online parameterization methodology and an adaptive observer are designed based on a cylindrical battery thermal model in this paper. The single cell thermal model is then scaled up to create a battery cluster model to investigate the temperature pattern of the cluster. The modeled thermal interconnections between cells include cell to cell heat conduction and thermal dynamics of the coolant flow due to convection. An observability analysis is performed on the cluster in order to design a closed loop observer. Based on the analysis, guidelines for sensor deployment are derived that guarantee observability of all temperature states.*
Keywords: lithium ion battery, core temperature, adaptive estimation, sensor deployment.

INTRODUCTION

Lithium-Ion (Li-ion) batteries are attractive energy storage devices for many hybrid electric vehicles (HEV) due to their high specific power and energy density compared with other batteries such as NiMH and Lead Acid. However, they typically have a constrained window of operating temperatures, around $-10 - 50^{o}C$. This constraint poses a unique cooling challenge for vehicles that operate in a very wide temperature range of $-46 - 72^{o}C$, or have active cooling limitations due to volume or weight constraints.

When batteries are operated outside their nominal temperature range, e.g. during overheating or operating in elevated temperatures, their lifespan and storage capacity are reduced, and performance degrades (Nguyen, 2004). An accurate prediction of battery thermal dynamics is the key to an effective thermal management system and to maintain safety, performance, and life longevity of these Li-Ion batteries (Mi, 2007).

Thermal modeling and management of batteries have received considerable attention in the past (Wang, 2002; Hallaj, 1999; Maleki, 2003; Gu, 2000; Mahamud, 2011; Smith, 2006; Bernardi, 1985). Some of those works could model detailed temperature distribution throughout the cell (Wang, 2002; Hallaj, 1999; Maleki, 2003; Gu, 2000), but they are generally computationally intensive and thus not suitable for onboard battery thermal management. Some of them tend to treat the battery as a whole and use one single temperature to capture the lumped thermal behavior of the cell (Gu, 2000; Mahamud, 2011; Smith, 2006; Bernardi, 1985) under certain conditions. However, significant difference between the surface and the core temperatures of a cell can be observed (Forgez, 2010), especially when the battery is operating under high C-rate. The temperature in the core of the cell can be much higher than in the surface (Forgez, 2010), and it is in the core where major battery thermal breakdown and degradation occur. Since direct measurement of the temperature can only be performed on the surface of the cell, a battery thermal model is desirable for estimating the battery core temperature T_c based on the measurement of the surface temperature T_s.

First and second order lumped thermal models for cylindrical lithium ion batteries have been proposed in Park (2003) and Forgez (2010). Such simplified models capture both the surface and core temperatures of the cell, and are efficient enough for onboard application. In order for the observer to work well, the model parameters should be as accurate as possible. Since all these parameters are lumped parameters for a simplified structure, textbook values found by correlating to the geometry of the battery and physical properties of all its components (Park, 2003) may not be accurate. The parameters can also be determined based on data obtained from designed experiments in a offline fashion (Park, 2003; Forgez, 2010). However, there could be two major disadvantages with such practice. On one hand, since the parameters are usually geometry and chemistry dependent, every time when the model is applied to a new type of battery, designed experiments will have to be conducted over again. On the other hand, some of the critical parameters, such as the internal resistance, may change over battery lifetime due to degradation, and thus should be identified continuously.

In order to address such problems, an online parameter identification scheme is designed in this paper. It can automatically identify the thermal model parameters without human interference, based on the current and surface temperature of the battery, which are the commonly measured signals in a vehicle battery management system. It is shown that the current of real drive cycles will be enough for the identification with no additional excitation needed. An adaptive observer is then designed to adopt the identified parameters for temperature estimation. The online identification scheme is capable of tracking the varying parameters,

either by resetting itself periodically over the battery lifetime, or by using forgetting factors (resolved in a separate publication (Lin, 2012)). Consequently, it not only ensures that the temperature estimation will not be affected by parameter drift due to degradation, but also can be used as a way to detect degradation.

Applications such as HEV's usually have hundreds, or even thousands, of battery cells in series and in parallel to meet their high power and voltage requirements. The cells are usually clustered in modules with specific electric and thermal connections. The temperatures for cells in a pack can vary significantly (Mahamud, 2011; Mi, 2007), due to pack geometry, cooling conditions and etc. As a result, it is desirable to monitor the temperatures of all the cells in the pack, which is, however, not economically feasible. Therefore, a thermal model for the battery cluster is developed in this paper by scaling up the single cell model with thermal interconnections between cells. Based on the thermal model, an observer can be designed to estimate all the core and surface temperatures with the knowledge of the measured input current, coolant flow rate, coolant inlet temperature, and strategically placed surface temperature measurements. Finally a sensor deployment strategy based on the observability conditions of the pack model is developed and the minimum number of required sensors can be investigated.

1 LUMPED THERMAL MODEL OF A CYLINDRICAL LITHIUM ION BATTERY

A cylindrical battery is here modeled with two states (Park, 2003), one for the surface temperature T_s and the other for the core temperature T_c, as shown in Figure 1.

The governing equations for the single cell thermal model are defined as in Park (2003),

$$\begin{cases} C_c \frac{dT_c}{dt} = I^2 R_e + \frac{T_s - T_c}{R_c} \\ C_s \frac{dT_s}{dt} = \frac{T_f - T_s}{R_u} - \frac{T_s - T_c}{R_c}. \end{cases} \tag{1}$$
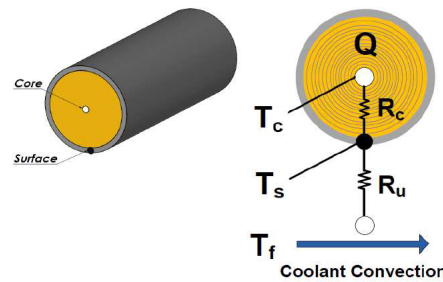

Figure 1

Single cell lumped resistance thermal model.

In this model, heat generation is approximated as a concentrated Joule loss in the battery core based on the simplified structure, computed as the product of the current I square by an internal resistance R_e. In addition, R_e can also be both temperature and state of charge (SOC) dependent and different for charging and discharging. For simplicity, it is here considered as a constant, and the more complicated varying R_e is addressed in another publication (Lin, 2012).

Heat exchange between the core and the surface is modeled by heat conduction over a thermal resistance, R_c, which is a lumped parameter including both the conduction and contact thermal resistance. A convection resistance R_u is modeled between the surface and the surrounding coolant to account for convective cooling. T_f is the temperature of coolant. R_u is actually a nonlinear function of the flow rate of the surrounding coolant, and in some vehicle battery systems, the coolant flow rate is adjustable to control the battery temperature. Here, it is considered as a constant as if the coolant flow rate is fixed to accommodate the maximum required cooling capacity. A Model with the more complicated varying R_u has also been investigated in (Lin, 2012). The rates of temperature change of the surface and the core depend on their respective lumped heat capacity C_s and C_c, where C_c is the heat capacity of the jelly roll inside the cell, and C_s is related to the heat capacity of the battery casing.

The complete parameter set for this model includes C_c, C_s, R_e, R_c, and R_u. Model identification techniques are to be developed to obtain precise values for the parameters based on measurable inputs and outputs.

2 PARAMETERIZATION METHODOLOGY

For linear model identification, a parametric model

$$z = \theta^T \phi \qquad (2)$$

should be derived first by applying Laplace transformation to the model, where z is the observation, θ is the parameter vector and ϕ is the regressor (Ioannou, 1996). Both z and ϕ should be measured signals.

With a parametric model available, various algorithms can be chosen for parameter identification, such as the gradient search and the least squares. The method of least squares is preferred here due to its advantages in noise reduction (Ioannou, 1996), which can be applied in either a recursive or a non-recursive form.

The non-recursive least squares is performed offline after all the experimental data have been taken over a time period $t_1, t_2, ..., t$, and the parameters can be calculated by (Ioannou, 1996)

$$\theta(t) = (\Phi^T(t)\Phi(t))^{-1} \Phi(t)Z(t), \qquad (3)$$

where

$$\begin{cases} Z(t) = [\frac{z(t_1)}{m(t_1)} & \frac{z(t_2)}{m(t_2)} & \cdots & \frac{z(t)}{m(t)}]^T \\ \Phi(t) = [\frac{\phi^T(t_1)}{m(t_1)} & \frac{\phi^T(t_2)}{m(t_2)} & \cdots & \frac{\phi^T(t)}{m(t)}]^T \\ m(t) = \sqrt{1 + \phi^T(t)\phi(t)}. \end{cases} \qquad (4)$$

The normalization factor m(t) is used to enhance the robustness of parameter identification.

The recursive least squares algorithm is applied in an online fashion, where parameters are updated at each time step by (Ioannou, 1996)

$$\begin{cases} \dot{\theta}(t) = P(t)\frac{\epsilon(t)\phi(t)}{m^2(t)} \\ \dot{P}(t) = -P(t)\frac{\phi(t)\phi^T(t)}{m^2(t)}P(t) \\ \epsilon(t) = z(t) - \theta^T(t)\phi(t) \\ m^2(t) = 1 + \phi^T(t)\phi(t), \end{cases} \qquad (5)$$

where P is the covariance matrix, and ϵ is the error in observation.

The recursive least squares algorithm can track time-varying parameters in real-time if forgetting factors are used and thus it gives the potential benefit of monitoring battery aging by tracking parameters that might change due to degradation, e.g. internal resistance.

In some cases, the observation z and the regressors ϕ in Eq. (2) may not be proper or causal, which means that the order of the denominator is lower than that of the numerator, and thus a filter $\frac{1}{\Lambda(s)}$ will have to be designed and applied to each signal to make it proper. The parametric model will then become

$$\frac{z}{\Lambda} = \theta^T \frac{\phi}{\Lambda}. \qquad (6)$$

3 PARAMETERIZATION OF THE CYLINDRICAL BATTERY THERMAL MODEL

In this section, a parameterization scheme will be designed for the cylindrical battery thermal model based on the methodology discussed previously.

According to Eq. (1), the inputs of the model are the current I and the coolant temperature T_f, and the measurable output is the battery surface temperature T_s. A parametric model for identification can be derived from Eq. (1) by performing Laplace transformation and substituting unmeasured T_c by measurable I, T_f and T_s,

$$\begin{aligned} s^2 T_s = &\frac{R_e}{C_c C_s R_c}I^2 + \frac{1}{C_c C_s R_c R_u}(T_f - T_s) \\ &- \frac{C_c + C_s}{C_c C_s R_c}s T_s + \frac{1}{C_s R_u}s(T_f - T_s). \end{aligned} \qquad (7)$$

In a real vehicle battery cooling system, the coolant temperature T_f will not necessarily be used as a controlled

input, and thus I may be the only rich excitation for identification. Consequently, sT_f becomes zero and the parametric model will be

$$
\begin{aligned}
s^2 T_s =& \frac{R_e}{C_c C_s R_c} I^2 + \frac{1}{C_c C_s R_c R_u}(T_f - T_s) \\
& - \left(\frac{C_c + C_s}{C_c C_s R_c} + \frac{1}{C_s R_u} \right) s T_s.
\end{aligned}
\tag{8}
$$

Since the initial battery surface temperature $T_{s,0}$ is not likely to be zero in most cases, initial conditions need to be incorporated, which gives

$$
\begin{aligned}
s^2 T_s - s T_{s,0} =& \frac{R_e}{C_c C_s R_c} I^2 + \frac{1}{C_c C_s R_c R_u}(T_f - T_s) \\
& - \left(\frac{C_c + C_s}{C_c C_s R_c} + \frac{1}{C_s R_u} \right) (s T_s - T_{s,0}).
\end{aligned}
\tag{9}
$$

A filter will be designed and applied later to make the parametric model proper.

For the parametric model in Eq. (9), the observation $z = s^2 T_s - s T_{s,0}$, the independent regressors $\phi = [I^2 \quad T_f - T_s \quad s T_s - T_{s,0}]^T$, and the parameter vector $\theta = [\alpha \quad \beta \quad \gamma]^T$, where $\alpha = \frac{R_e}{C_c C_s R_c}$, $\beta = \frac{1}{C_c C_s R_c R_u}$ and $\gamma = - \left(\frac{C_c + C_s}{C_c C_s R_c} + \frac{1}{C_s R_u} \right)$.

By using parametric model Eq. (9), only the three lumped parameters, α, β and γ, can be identified under the condition of persistent input excitation (Ioannou, 1996). It is insufficient to determine a set of unique solution for the original five physical parameters, C_c, C_s, R_e, R_c, and R_u, by simply knowing α, β and γ since the number of equations is less than the number of variables. Therefore, prior knowledge of two of the physical parameters should be assumed in order to obtain the unique parameter set.

Of the five physical parameters, the internal resistance R_e may vary due to aging. The thermal resistance R_c is difficult to measure, because it is a lumped parameter including both conduction and contact resistance; the convection resistance R_u will be influenced by the coolant flow conditions around the cell. Therefore, it is not easy to obtain prior knowledge of those three parameters. The heat capacities C_c and C_s, which depend on the thermal properties and the mass of the jelly roll and the casing, are relatively constant over lifetime. In addition, the heat capacities will only affect the speed of transient response of the model without having any impact on the steady state temperatures. Consequently, the heat capacities C_c and C_s are selected to be the presumed parameters.

With C_c and C_s presumed and α, β and γ identified, R_e, R_c and R_u can be obtained by

$$
\begin{cases}
(C_c + C_s) C_s \beta R_u{}^2 + C_s \gamma R_u + 1 = 0 \\
R_c = \frac{1}{\beta C_s C_c R_u} \\
R_e = C_c C_s \alpha R_c.
\end{cases}
\tag{10}
$$

The quadratic equation for R_u in Eq. (10) will possibly give two solutions, but the right one can be decided by a rough estimation on the coolant flow conditions.

A second order filter should be applied to the observation and the regressors in Eq. (9) to make them proper. The filter takes the form

$$
\frac{1}{\Lambda(s)} = \frac{1}{(s + \lambda_1)(s + \lambda_2)},
\tag{11}
$$

where λ_1 and λ_2 are designed based on the input and system dynamics.

The least squares algorithm in Eq. (3) and Eq. (5) can then be applied to implement model identification.

4   ADAPTIVE OBSERVER DESIGN

In this section, an adaptive observer which can perform online parameter and state estimation simultaneously is designed based on the recursive least squares model identification scheme and a model observer.

It is a common practice to design a closed loop observer, such as a Luenberger observer or a Kalman filter, to estimate the unmeasurable states of a system based on measurable output and a model. The closed loop observer is similar to the closed loop controller, but is used for state estimation instead of feedback control. The observer for a linear system

$$
\begin{cases}
\dot{x} = Ax + Bu \\
y = Cx + Du
\end{cases}
\tag{12}
$$

takes the form (Williams, 2007)

$$
\begin{cases}
\dot{\hat{x}} = A\hat{x} + Bu + L(y - \hat{y}) \\
\hat{y} = C\hat{x} + Du,
\end{cases}
\tag{13}
$$

where x and y are the actual system states and output, $\hat{x}$ and $\hat{y}$ are estimated states and output, L is the observer gain, and A, B, C and D are model parameters. The difference between the measured and the estimated output is used as a feedback to correct the estimated states. The closed loop observer has certain advantages over the open loop observer (observer without output feedback). It can guarantee fast convergence of the estimated states to those of the real plant under uncertain initial conditions, e.g. a Luenberger observer (Williams, 2007), or optimize the estimation by balancing the effect of process and measurement noises, e.g. a Kalman filter (Kalman, 1960).

The cylindrical battery thermal model described by Eq. (1) can be written in state space form as

$$
\begin{cases}
x = [T_c \quad T_s]^T, \quad y = T_s, \quad u = [I^2 \quad T_f]^T \\
A = \begin{bmatrix} -\frac{1}{R_c C_c} & \frac{1}{R_c C_c} \\ \frac{1}{R_c C_s} & -\frac{1}{C_s}(\frac{1}{R_c} + \frac{1}{R_u}) \end{bmatrix} \\
B = \begin{bmatrix} \frac{R_e R_c}{C_c} & 0 \\ 0 & \frac{1}{R_u C_s} \end{bmatrix} \\
C = [0 \quad 1] \\
D = 0.
\end{cases}
\tag{14}
$$

An adaptive observer is designed based on certainty equivalence principle (Ioannou, 1996), where the estimated parameters from online identification in Eq. (5) are adopted for the observer. The structure of the whole online identification scheme and adaptive observer is shown in Figure 2.

As shown in Figure. 2, when the thermal management system is operating in real time, the input current I, coolant temperature T_f and the measured surface cell temperature T_s are fed into the parameter identifier to estimate model parameters R_u, R_e and R_c. The adaptive observer, on one hand, adopts the estimated parameters for temperature estimation. On the other hand, it takes the errors between the measured and the estimated T_s as a feedback to correct its core and surface temperature estimation. Estimations of both parameters and temperatures are updated at each time step.

5 SIMULATION FOR PARAMETERIZATION AND ADAPTIVE OBSERVER FOR A CYLINDRICAL BATTERY THERMAL MODEL

Simulation has been conducted to verify the designed parameterization scheme and adaptive observer. A cylindrical battery thermal model in Eq. (1) with parameters of an $A123$ 32157 $LiFePO4$/graphite battery is used to generate data for methodology verification. Parameters are assumed by taking or scaling up relevant parameters in Forgez (2010) and A123 datasheet, or being calculated based on Incropera (1985). The values of the model parameters are listed in Table 1.

The coolant considered here is air, and $R_u = 0.79 KW^{-1}$ corresponds to an air flow of $9.5 \times 10^{-3} m^3/s^{-1}$ around a 32157 cell. The air flow temperature is fixed at 25^oC. The main purpose of the simulation is to check whether the

designed algorithm can be applied to identify parameters and estimate core temperature T_c, and thus the values of the assumed model parameters are not of essential importance.

A driving cycle with high power excursion for army application, Urban Assault Cycle (UAC) (Lee, 2011), is adopted as the current excitation, as shown in Figure 3. The vehicle velocity profile of UAC is plotted in Figure 3, and the current load for the battery system is calculated for a 13.4 ton armored military vehicle in Lee (2011), as shown in Figure 3. As one can see that the UAC involves up to 20C battery discharging and 12C charging, which includes the current from regenerative braking. Repeated UAC cycles are used as the model input to generate the surface temperature T_s to test the identification scheme. The core temperature simulated by the model is recorded for verification. The urban assault cycle current profile I and the simulated T_s are shown in Figure 3. The three parameters to be identified, R_u, R_c and R_e, are initialized to be

$$R_e^0 = 10m\Omega \quad R_c^0 = 2KW^{-1} \quad R_u^0 = 1.5KW^{-1}, \quad (15)$$

which are different from the nominal values in Table 1.

The online identification results are plotted in Figure 4. It can be seen that all the three parameters converge to the nominal values in Table 1, despite starting at some random

TABLE 1

Nominal model parameters.

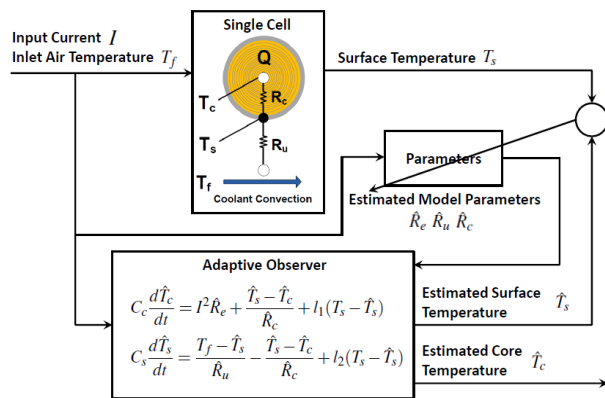| Parameters	Values
C_c	$268 JK^{-1}$
C_s	$18.8 JK^{-1}$
R_e	$3.5m\Omega$
R_c	$1.266 KW^{-1}$
R_u	$0.79 KW^{-1}$

Figure 2

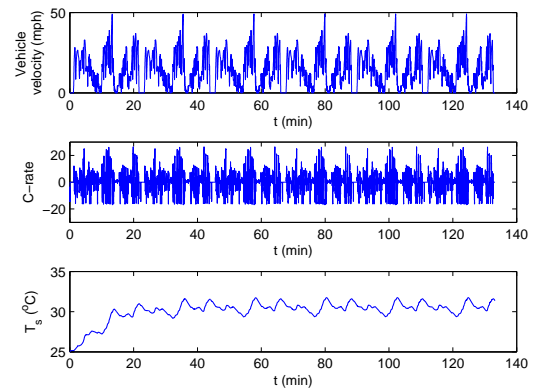Online identification scheme and adaptive observer structure.

Figure 3

Simulated drive cycle and surface temperature output for verification.

initial values. Both the identified R_e and R_c converge within 10 minutes whereas R_u takes longer. The response of the adaptive observer is plotted in Figure 5. In Figure 5, the temperatures T_c and T_s simulated by the model that emulates the real battery are presented and the estimated T_c and T_s are plotted to evaluate the performance of the adaptive observer. The simulated core temperature T_c and surface temperature T_s are initialized to be 25^oC and the adaptive observer is preset to start from 10^oC for both temperatures. It is noted that the estimated surface temperature converges to the real values within 20 minutes, because the T_s is directly measured and fed back into the observer to force the observer to match the measurement. The estimation of the core temperature, T_c, instead, converges much slower (in about 60 minutes). This slower adaption occurs because T_c is not directly measured, and thus the estimation of T_c

will heavily depend on the precision of the model. As can be seen in Figure 4, since the parameters estimated by the identifier fluctuated for a while before finally converged to the correct values, the convergence of T_c estimation can only happen afterwards.

6 SCALABLE BATTERY CLUSTER THERMAL MODEL AND SENSOR DEPLOYMENT ANALYSIS

In vehicle application, batteries are usually packed in modules to satisfy the energy and power demand. This section is devoted to constructing a thermal model for a battery cluster based on the previously discussed single cell model. The cluster model can then be used to design an thermal observer for the cluster. The parameters identified by the online identifier discussed above can be updated in real time to the cluster model for adaptation. To optimize temperature estimation, a closed loop observer with surface temperature feedback is desirable, which will require observability. The observability analysis will then be conducted to the cluster thermal model to guide sensor deployment.

6.1 Scalable Battery Cluster Thermal Model

The single cell cylindrical battery thermal model in Eq. (1) can be scaled up to a battery cluster model by considering cell to cell heat conduction (Smith, 2009), and the heat balance of the flowing coolant (Park, 2003, 2011), as shown in Figure 6.

As shown in Figure 6, the cluster can be simplified by considering cells that are connected in series with tabs and are geometrically arranged in a row configuration along the
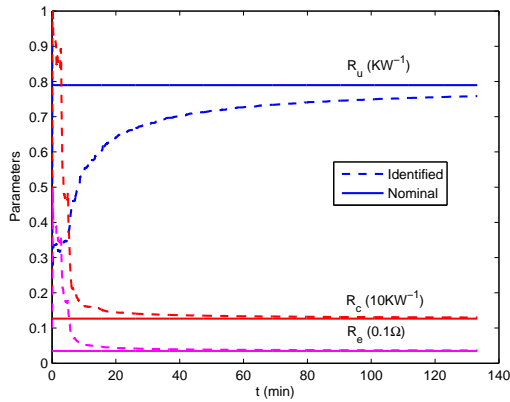

Figure 4

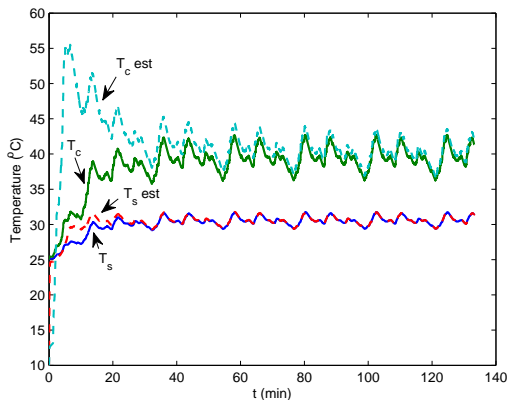Online paramter identification results.
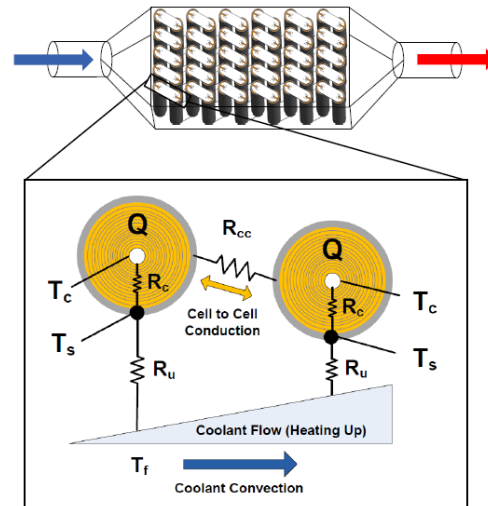

Figure 5

Adaptive observer response.

Figure 6

Battery pack configuration.

coolant flow path. The coolant flows through the space between cells from the inlet to the outlet, and picks up the heat dissipated from the cell surface through convection.

The temperature evolution of the kth cell in a cluster can be modeled as

$$\begin{cases} C_c \frac{dT_{c,k}}{dt} & = I^2 R_e + (T_{s,k} - T_{c,k})/R_c \\ C_s \frac{dT_{s,k}}{dt} & = \frac{T_{f,k} - T_{s,k}}{R_u} - \frac{T_{s,k} - T_{c,k}}{R_c} \\ & \quad + \frac{T_{s,k-1} + T_{s,k+1} - 2T_{s,k}}{R_{cc}} \\ T_{f,k} & = T_{f,k-1} + \frac{T_{s,k-1} - T_{f,k-1}}{R_u C_f}, \end{cases} \tag{16}$$

where k is the index of the cell along the coolant flow direction.

In Eq. (16), the heat conduction between cells is modeled as heat flow over the conduction resistance R_{cc}, driven by the temperature difference between the adjacent cell surfaces. It is noted here that R_{cc} is a lumped parameter, which may include heat conduction through the tab and other possible connections between cells depending on the cluster structure. The coolant flow temperature of the kth cell, $T_{f,k}$, is determined by the flow heat balance of the previous cell, which is calculated by dividing the heat removed $\frac{T_{s,k-1} - T_{f,k-1}}{R_u}$ from the $k-1th$ cell by the coolant flow capacity C_f. Parameters are assumed to be equal for every cell and the current is also the same for each cell since the cluster is in series connection.

The temperature profile for a cluster with 5 cells subject to Urban Assault Cycle is shown in Figure 7. $Cell_1$ is close to the coolant inlet while $Cell_5$ is close to the outlet. The surrounding air temperature for this simulation is set at 25^oC and the flow rate is $9.5 \times 10^{-3} m^3 s^{-1}$, corresponding to a flow velocity of $1.515 ms^{-1}$.

Figure 7

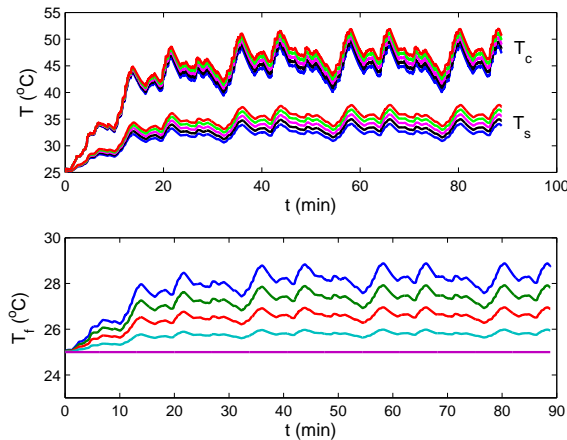Simulated battery pack temperature profile subject to UAC cycle (for T_c, T_s and T_f, from bottom to top: $Cell_1$, $Cell_2$, $Cell_3$, $Cell_4$, $Cell_5$).

In Figure 7, the coolant air temperature T_f for $Cell_1$ keeps constant at 25^oC since the inlet air temperature is controlled. As the coolant air flows from $Cell_1$ to $Cell_5$, its temperature T_f increases as it picks up the heat from the cells. Consequently, the surface and the core temperatures of the cells will also increase down the string towards the coolant outlet due to the coolant temperature rise.

Here, it is assumed that every single cell in the string has the same R_u, and thus the heat rejection capacity for each cell is the same. As can be seen in Figure 7, the hottest cell will be the last one because the difference in cooling among cells is only affected by the coolant temperature. For some pack geometries, it might be possible that different cells are subject to different flow conditions, e.g. the cells at the two ends of the string may have higher heat rejection capacity due to the larger space around them. Therefore, the cells in the middle of the string may have the highest temperatures. For those cases, different R_u numbers can be applied to different cells to capture these variations.

6.2 Battery Cluster Thermal Observer

Monitoring the temperature variation among cells in a battery pack is of great interest for pack thermal management. On one hand, it is always crucial to monitor the highest cell temperatures in a pack to prevent overheating and its disastrous outcomes. On the other hand, the battery performance will be different under different temperatures, such as the internal resistance, efficiency, self-discharging rate, degradation rate and etc. Hence, imbalances in cell voltage, state of charge (SOC) and state of health (SOH) may exist among cells in the cluster. There have been quite some efforts to alleviate or compensate for such imbalance, and observing the temperature variation beyond normal levels among cells in a battery pack can provide basis for such attempts.

In a commercial battery module for automotive application, there are usually hundreds or even thousands of cells in total, and it is not quite possible to measure the surface temperature for every single cell. One of the common practice is to test the pack before installation and identify those cells with the highest temperature under experiment conditions, and thermocouples will be mounted on those cells to monitor the critical temperatures as a reference for cooling control and power management.One potential issue with such method is that it cannot obtain the temperatures of every single cell and hence capture the thermal non-uniformity across the pack. Consequently, model based temperature monitoring might be highly desirable since it can estimate the core temperature T_c and the surface temperature T_s of every cell in the pack.

The cluster thermal model developed in this paper can be used for cluster thermal monitoring. A model based state estimator can be categorized as either an open loop observer or a closed loop observer. As for an open loop observer, the

estimated states are calculated by the model solely based on the inputs. In this case specifically, the current and the coolant inlet temperature are measured and applied to the battery pack thermal model in Eq. (16) to calculate all the temperatures in the pack. The open loop observer will give accurate state estimation if the initial conditions of all the states are known.

When the initial conditions are not available, the estimated states will still converge to the real states gradually if the system is stable, but the converging speed will depend on the system dynamics. The battery thermal model here is stable since all its states will gradually decay to zero subject to zero input. However, when the initial core and the surface temperatures of the cells are not known, the estimated temperatures will converge very slowly to the real temperatures due to the slow thermal dynamics of the battery.

The unknown initial temperatures can be a problem under some circumstances. Since the temperature sensors can only be installed on cell surfaces, only the initial surface temperatures can be obtained precisely at startup while the initial core temperatures remain unknown. If the vehicle is started from steady states, e.g. after overnight rest, the unmeasured initial core temperatures of the cells can be assumed to be the same as the measured initial surface temperatures. But such an assumption may not be valid for short shutdown. Figure 8 shows the simulated temperature evolution during shutdown of a battery pack with 5 cells in series. The temperature profile of the precedent operation cycle is shown in Figure 7. The current is cut off at the beginning of the simulation in Figure 8 as the shutdown is initiated, and the cooling system is kept on during the shutdown process.

It can be observed in Figure 8 that it takes the battery pack more than 40 minutes to reach steady state, when the cells are completely cooled down and thus surface temperatures T_s and the core temperatures T_c are equal. In real application, since it may not be feasible to keep the cooling system on for 40 minutes after key-off, the actual time for the pack to reach steady state will be longer. If the driver tries to turn the vehicle back on before the pack gets to thermal equilibrium, the initial reading of the surface temperature at startup will not be a good approximation for the initial core temperatures. The shorter the shutdown is, the larger the errors of such approximation will be. For example, if the next startup occurs at about 10 minutes after the previous shutdown, according to Figure 8, the difference between the surface and the core temperatures will be roughly 7^oC.

Simulation has been conducted to investigate how fast the open loop estimation of the temperatures will converge under such errors in initial conditions. In simulation, the real initial surface and core temperatures of all the cells are set to be 30^oC and 37^oC respectively. For the open loop observer, the initial core temperatures are assumed to be

the same as the measured surface temperatures, which are 30^oC. The results are shown in Figure 9. For clarity, only the temperatures of $Cell_1$ and $Cell_5$ are plotted.

It can be observed in Figure 9 that it takes the open loop estimation more than 30 minutes to roughly converge to the real surface and core temperatures for both $Cell_1$ and $Cell_5$. Such a big delay is due to the slow thermal dynamics of the batteries and may lead to ineffective battery management during the startup period. It is noted that in onboard battery management system, not every cell surface temperature is measured. As a result, in addition to the unknown core temperatures considered here, the surface temperatures of those unmeasured cells will also be unknown at startup. Such uncertainty may further increase the delay of convergence.

In order to minimize delay in estimation due to unknown initial temperatures, a closed loop observer can be designed to achieve fast estimator convergence. For a closed loop observer, besides the inputs, some of the states or state-related variables are also measured and the errors between the measurement and the estimation are fed back to the observer to correct the model estimation (Williams, 2007), as shown in Eq. (13). If the model is completely observable, by tuning the observer gains, the dynamics of the closed loop observer can be designed to be fast and the estimated temperatures will converge to the real plant temperatures much more quickly than the open loop estimation when starting from unknown initial temperatures.

Simulation for a closed loop temperature observer is shown in Figure 9 to compare with the performance of the open loop observer. In Figure 9 that although starting from the same erroneous initial guess of the core temperatures, the closed loop estimation converge to the real temperatures
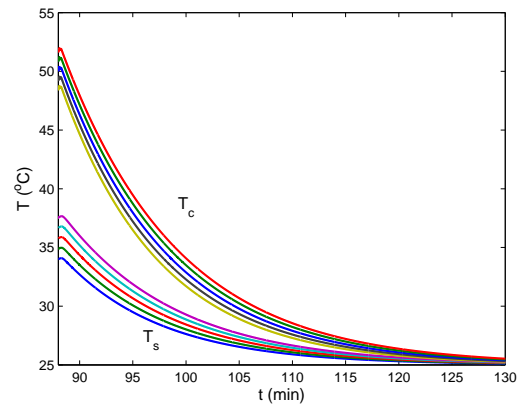
Figure 8

Simulated battery pack temperature profile during shutdown (for T_c, T_s and T_f, from bottom to top: $Cell_1$, $Cell_2$, $Cell_3$, $Cell_4$, $Cell_5$).

much faster than the open loop estimation. Both temperatures estimated by the closed loop observer converge to the real temperatures almost instantly, as compared to the 30 minutes taken by the open loop observer. It is noted that simulation in Figure 9 assumes known parameters for all the cells, which are identified by the previous single cell identifier. That is why the estimated temperatures can converge instantly.

Since only when the system is observable could the closed loop observer be tuned arbitrarily fast, a new method for temperature sensor deployment can be studied by investigating the observability conditions for the battery cluster model.

6.3 Investigation on Sensor Deployment based on Cluster Model Observability Analysis

The observability of a model can be examined by its observability matrix

$$Q = \begin{bmatrix} C \\ CA \\ \cdots \\ CA^{n-1} \end{bmatrix}, \qquad (17)$$

where A is the system matrix and C is the output matrix in Eq. (12), and n is the order of the system. The model will be completely observable if and only if the rank of Q is equal to n.

First, a battery string with 2 cells is investigated for simplicity. Based on Eq. (16), for a battery string with 2 cells, we have

$$\begin{bmatrix} \dot{T}_{c,1} \\ \dot{T}_{s,1} \\ \dot{T}_{c,2} \\ \dot{T}_{s,2} \end{bmatrix} = A \begin{bmatrix} T_{c,1} \\ T_{s,1} \\ T_{c,2} \\ T_{s,2} \end{bmatrix} + \begin{bmatrix} \frac{R_e}{C_c} & 0 \\ 0 & \frac{1}{R_u} \\ \frac{R_e}{C_c} & 0 \\ 0 & 0 \end{bmatrix} \begin{bmatrix} I^2 \\ T_{f,in} \end{bmatrix} \qquad (18)$$

with A specified in Eq. (19).

In Eq. (19), the $\frac{1}{R_{cc}C_s}$ terms in the $2nd$ and the $4th$ row of the A matrix reflect the thermal interaction between the 2 cells through cell to cell conduction. The $\frac{1}{R_u{}^2 C_f C_s}$ term in the $4th$ row represents the impact of the first cell on the second one through coolant flow convection. The absence of this term in the $2nd$ row indicates that such impact is unidirectional and the second cell cannot influence the first cell via coolant convection.

The C matrix will be determined by the location of the sensor. If the surface temperature of $Cell_1$ is measured, then $C_1 = \begin{bmatrix} 0 & 1 & 0 & 0 \end{bmatrix}$, and if the surface temperature of $Cell_2$ is measured, $C_2 = \begin{bmatrix} 0 & 0 & 0 & 1 \end{bmatrix}$.

If all the elements in A are assigned with the values assumed in this paper and applied to Eq. (17) to calculate Q, it can be found that the rank of Q will be 4 when either C_1 or C_2 is applied. This means that for a cell string with
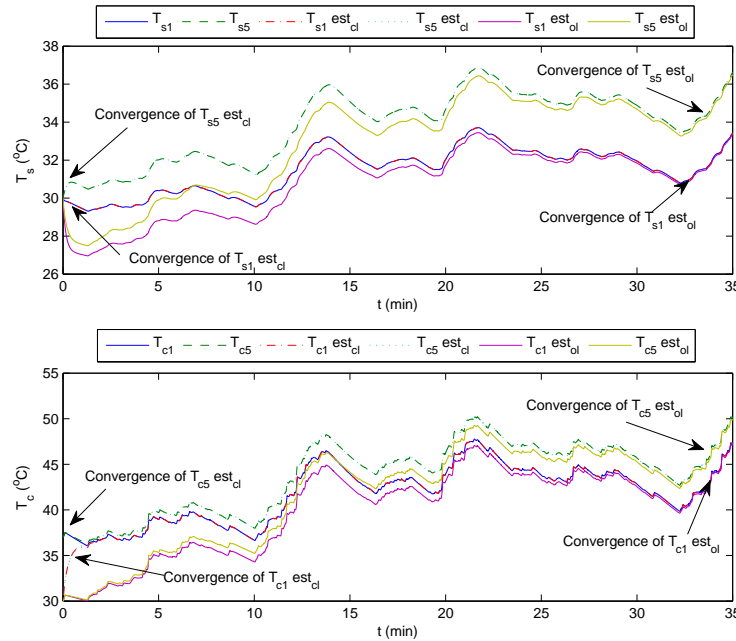

Figure 9

Convergence of open loop and closed loop observer

$$A = \begin{bmatrix} -\frac{1}{R_cC_c} & \frac{1}{R_cC_c} & 0 & 0 \\ \frac{1}{R_cC_s} & -(\frac{1}{R_cC_s} + \frac{1}{R_uC_s} + \frac{1}{R_{cc}C_s}) & 0 & \frac{1}{R_{cc}C_s} \\ 0 & 0 & -\frac{1}{R_cC_c} & \frac{1}{R_cC_c} \\ 0 & (\frac{1}{R_u{}^2C_fC_s} + \frac{1}{R_{cc}C_s}) & \frac{1}{R_cC_s} & -(\frac{1}{R_uC_s} + \frac{1}{R_cC_s} + \frac{1}{R_{cc}C_s}) \end{bmatrix}. \qquad (19)$$

2 cells, either measuring the first or the second cell will give full observability.

For a cell string with 3 cells in series, the A matrix can be established as Eq. (20). Similar to the A matrix for the 2 cell string in Eq. (19), the $\frac{1}{R_{cc}C_s}$ terms in the $2nd$, $4th$ and $6th$ rows reflect the interaction between the adjacent cells via cell to cell heat conduction, and the $\frac{1}{R_u{}^2C_fC_s}$ term in the $4th$ row accounts for the impact of the first cell on the second cell by coolant flow convection. More details about the cell interconnection via coolant convection can be revealed by exploring the $6th$ row of the A matrix. In the $6th$ row, the $\frac{1}{R_u{}^2C_fC_s}$ term in the $4th$ column represents the impact of the second cell on the third cell through coolant convection and the $\frac{1}{R_u{}^2c_fc_s} - \frac{1}{R_u{}^3c_f{}^2c_s}$ term in the $2nd$ column describes such impact of the first cell on the third cell. It can be seen that all the previous cells in the string will affect the subsequent cells through coolant flow convection, and the further apart the two cells are, the weaker such effect will be. Such feature of the coolant convection is different from that of the cell to cell conduction, which only exists between adjacent cells and the strength is always the same.

For cell strings with any number of cells, after establishing the A matrix similar to Eq. (19) and Eq. (20), observability analysis can be conducted to find the minimum number of sensors that gives full observability. The results are summarized in Table 2.

It is noted that for cell strings with more than 5 cells, the sensor location will also have an effect on the observability. For example, for a string with 5 cells, although the minimum number of sensors for full observability is 2, different sensor locations may lead to different results on observability, as shown in Figure 10. It can be seen that if the 2 sensors are placed at the first 2 cells, the rank of the Q matrix will be less than 10 and thus the full observability cannot be satisfied. But when the 2 sensors are placed at the first cell and the last cell, the Q matrix will be of full rank and thus gives full observability. This can be explained by the

essence of the observability. Observability actually indicates the possibility of determining all the states based on the available measurements and the model. The model defines the relations between different states and thus in order to achieve full observability, the measurements should be able to provide enough constraints to restrict the states to a single set of solution based on the model. When the sensors are placed at the first 2 cells, the constraints provided by the sensors are redundant at the beginning section of the string, since the surface temperature of the second cell can be calculated based on the measured surface temperature of the first cell and the model. However, because there is no measurement in the latter section of the string, the temperatures of the cells in that section cannot be constrained to unique values. Consequently, the condition of full observability is not satisfied. When the sensors are deployed at the first and the last cells, constraints are imposed on the string evenly, and thus all the states can be determined by the measurements and the model.

In some cases, the thermal interconnections between the cells may be weaker if either cell to cell heat conduction or coolant convection is missing or negligible. For one thing, cell to cell conduction can be very small in some pack designs due to the shape or the material of the tab. For another, when the coolant flow is not circulated through the pack, e.g. during cooling system breakdown, the cells will be cooled via natural convection and the previous cells will not affect the subsequent cells through coolant convection. Under these

TABLE 2

Minimum number of sensors for a battery string

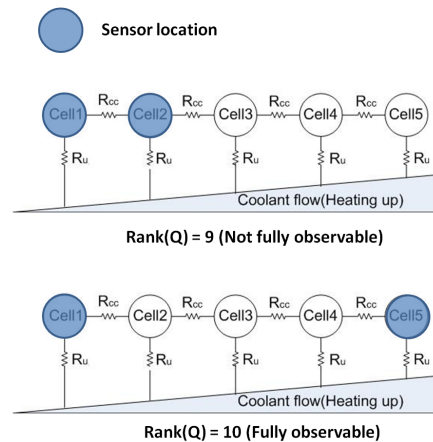| No. of cells	Min. No. of sensors
1,2,3	1
4,5,6	2
7,8,9	3
10,11,12	4

Figure 10

Sensor location determines full observality.

$$A_{-3cell} = \begin{bmatrix} -\frac{1}{R_c c_c} & \frac{1}{R_c c_c} & 0 & 0 & 0 & 0 \\ \frac{1}{R_c c_s} & -(\frac{1}{R_c c_s} + \frac{1}{R_u c_s} + \frac{1}{R_{cc} c_s}) & 0 & \frac{1}{R_{cc} c_s} & 0 & 0 \\ 0 & 0 & -\frac{1}{R_c c_c} & \frac{1}{R_c c_c} & 0 & 0 \\ 0 & \frac{1}{R_u{}^2 c_f c_s} + \frac{1}{R_{cc} c_s} & \frac{1}{R_c c_s} & -(\frac{1}{R_u c_s} + \frac{1}{R_c c_s} + \frac{2}{R_{cc} c_s}) & 0 & \frac{1}{R_{cc} c_s} \\ 0 & 0 & 0 & 0 & -\frac{1}{R_c c_c} & \frac{1}{R_c c_c} \\ 0 & \frac{1}{R_u^2 c_f c_s}(1 - \frac{1}{R_u c_f}) & 0 & \frac{1}{R_u{}^2 c_f c_s} + \frac{1}{R_{cc} c_s} & \frac{1}{R_c c_c} & -(\frac{1}{R_c c_s} + \frac{1}{R_u c_s} + \frac{1}{R_{cc} c_s}). \end{bmatrix} \quad (20)$$

circumstances, the observability conditions will be different. Take a cell string with 5 cells as an example. As shown in Figure 11, when the coolant circulation is disabled and the cells are cooled by natural convection, placing the sensors at the first and the last cell can still satisfy observability condition. But when the cell to cell conduction is missing, the same sensor locations cannot give full observability.

Such discussion can be generalized to strings with more cells. A string with 12 cells is analyzed and the results are summarized in Table 3. The minimum number of sensors that gives full observability is 4. As shown in Table 3, among all the 495 combinations of 4 sensor locations in a cell string of 12, if there are both circulated coolant convection and cell to cell conduction, referred to as full interconnection in

Table 3, 106 combinations will give full observability. Under natural convection, where the coolant is not flowing between cells, only 52 combinations can satisfy full observability condition. When the cell to cell conduction is missing, only 1 combination yields full observability. That combination would be evenly distributing the sensors at the $3th$, $6th$, $9th$ and $12th$ cells, which quite agrees with intuition.

Of the two modeled thermal interconnections between cells, namely the cell to cell heat conduction and the heat convection through the coolant flow, the former tends to have larger impact on the observability of the pack model. This may be related to the fact that the cell to cell heat conduction is a two-way interaction, whereas the heat convection through the coolant flow is single directional.

Consequently, greater cell to cell heat conduction is favored by the observability of the pack model. It is noted that great cell to cell heat conduction can also reduce the temperature gradient between cells in the pack and thus help contain the imbalance between cells induced by temperature non-uniformity. However, on the negative side, in case of a single cell thermal failure, e.g. local overheating, the great cell to cell heat conduction will facilitate the spread of such failure to other cells in the pack, which is not desirable from the safety perspective.

CONCLUSION

In this paper, an online parameterization methodology for a lumped thermal model of a cylindrical lithium ion battery cell has been proposed, designed and verified by simulation. By using online parameterization algorithm, the lumped parameters of the thermal model, which cannot be easily measured or calculated otherwise, can be automatically identified based on the current excitation of a real drive cycle and the resultant battery surface temperatures. The identified parameters and the measured cell surface temperature are adopted by an adaptive observer to estimate the unmeasurable core temperature of the cell. The estimated core temperature can be used as a more useful and critical reference for the on-board thermal management system and even the vehicle power management system. The next step will be to validate the model and the methodology with experiments. Over the battery lifetime, such online identification scheme can be reset on a monthly or yearly basis
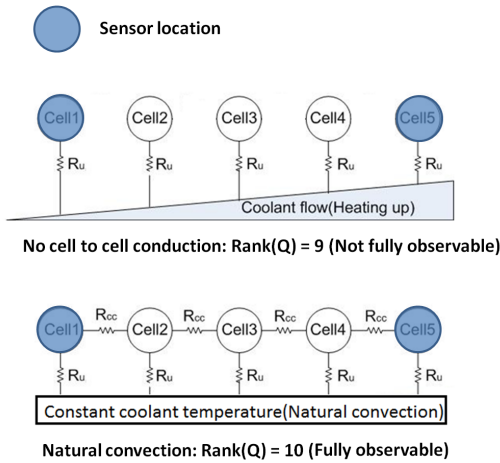

Figure 11

Observability of the same sensor locations under different conditions.

TABLE 3

Number of sensor position combinations giving full observability for a string with 12 cells and 4 sensors

Conditions	No. of combinations giving full observability
Full interconnection	106/495
Natural convection	52/495
No cell to cell conduction	1

Les Rencontres Scientifiques d'IFP Energies nouvelles – RHEVE 2011

to track varying parameters due to degradation. This can also be achieved by using forgetting factors, which has been explored in another publication (Lin, 2012).

The single cell model is then scaled up to a one-dimensional cluster model after being augmented with cell to cell heat conduction and coolant flow thermal dynamics due to convection. The cluster model can be further scaled to multi-dimensional models with more complicated thermal connections between cells. Different cooling strategies and configurations for the pack can be accommodated by tuning the values of the parameters. The observability of the cluster model is investigated to enlighten pack sensor deployment. The system matrix of the cluster model has been explored and minimum number of sensors required have been determined for clusters with various lengths. It is interesting to notice that the sensor locations will affect the observability of the cluster, and such impacts will be different for different cluster constructions and cooling conditions.

At this point, the adaptation of the cluster thermal monitoring is achieved by propagating the parameters identified online from a single cell to the whole cluster. The underlying assumption is that all the cells are behaving and degrading at the same pace. To achieve full adaptation of the cluster, where degradation profile can be established for the cluster, the sensor deployment will be investigated based on the identifiability analysis of the cluster model.

ACKNOWLEDGEMENTS

REFERENCES

[1] Nguyen, J. and Taylor, C. (2004) Safety Performance of a Large Format, Phosphate Based Lithium-Ion Battery. *26th Annual International Telecommunications Conference.*

[2] Mi, C., Li, B, Buck, D. and Ota, N. (2007) Advanced Electro-Thermal Modeling of Lithium-Ion Battery System for Hybrid Electric Vehicle Applications. *Vehicle Power and Propulsion Conference.*

[3] Wang, C.Y. and Srinivasan, V. (2002) Computational battery dynamics (CBD) − electrochemical/thermal coupled modeling and multi-scale modeling. *Journal of Power Sources.* **110**, 364-376.

[4] Hallaj, S. A., Maleki, H., Hong, J. and Selman, J. (1999) Thermal modeling and design considerations of lithium-ion batteries. *Journal of Power Sources.* **83**, 1-8.

[5] Maleki, H. and Shamsuri, A. K. (2003) Thermal analysis and modeling of a notebook computer battery. *Journal of Power Sources.* **115**, 131-136.

[6] Gu, W. B. and Wang, C. Y. (2000) Thermal analysis and modeling of a notebook computer battery. *Journal of Power Sources.* **115**, 131-136.

[7] Mahamud, R. and ChanwooPark. (2011) Reciprocating airflow for Li-ion battery thermal management to improve temperature uniformity. *Journal of Power Sources.* **196**, 5685-5696.

[8] Smith, K. and Wang, C. Y. (2006) Power and thermal characterization of a lithium-ion battery pack for hybrid-electric vehicles. *Journal of Power Sources.* **160**, 662-673.

[9] Bernardi, D., Pawlikowski, E. and Newman, J. (1985) A General Energy Balance for Battery Systems. *J. Electrochem. Soc..* **132**, 5-12.

[10] Forgez, C., Do, D. V., Friedrich, G., Morcrette, M. and Delacourt, C. (2010) Thermal modeling of a cylindrical LiFePO4/graphite lithium-ion battery. *Journal of Power Sources.* **195**, 2961-2968.

[11] Park, C. W. and Jaura, A. K. (2003) Dynamic Thermal Model of Li-Ion Battery for Predictive Behavior in Hybrid and Fuel Cell Vehicles. *SAE.* 2003-01-2286.

[12] Lin, X., Perez, H. E., Siegel, J. B., Stefanopoulou, A. G., Li, Y. and Anderson, R. D. (2012) Quadruple Adaptive Observer of Li-ion Core Temperature in Cylindrical Cells and their Health Monitoring. *2012 American Control Conference.* Submitted.

[13] Ioannou, P. A. and Sun, J. (1996) Adaptive Robust Adaptive Control. Prentice Hall.

[14] Williams R. L. II and Lawrence D.A. (2007) Linear state-space control systems. Wiley.

[15] Kalman, R. E. (1960) A New Approach to Linear Filtering and Prediction Problems. *Transactions of the ASME Journal of Basic Engineering.* **82**, 35-45.

[16] A123Systems Inc. (2006) A123 Systems Datasheet: High Power Lithium Ion ANR26650M1. www.a123systems.com.

[17] Incropera, F. and De Witt, D. (1985) Fundamentals of heat and mass transfer. John Wiley and Sons Inc.,New York, NY.

[18] Lee, T.-K., Kim, Y., Stefanopoulou, A. G. and Filipi, Z. (2011) Hybrid Electric Vehicle Supervisory Control Design Reflecting Estimated Lithium-Ion Battery Electrochemical Dynamics. *American Control Conference.*

[19] Smith, K., Kim, G.-H., Darcy, E. and Pesaran, A. (2009) Thermal/electrical modeling for abuse-tolerant design of lithium ion modules. *International Journal of Energy Research.* **34**, 204-215.